Neuroanatomical and behavioral characterization of corticotropin releasing factor-expressing lateral Habenula neurons in mice

William J. Flerlage[1,#], Shawn C. Gouty[1, #], Emily H. Thomas[1, #], Sarah C. Simmons[1], Mumeko C. Tsuda[2], Oana L. Rujan[1], Laxmi Iyer[3], Emily Petrus[4], Brian M. Cox[1], T. John Wu[5], Fereshteh S. Nugent[1].

[1]Uniformed Services University of the Health Sciences, Department of Pharmacology and Molecular Therapeutics, Bethesda, MD 20814, USA.

[2] Uniformed Services University of the Health Sciences, Preclinical Behavior and Modeling Core, Bethesda, MD 20814, USA.

[3]Henry M. Jackson Foundation for the Advancement of Military Medicine, Bethesda MD 20817

[4]Uniformed Services University of the Health Sciences, Department of Anatomy, Physiology, and Genetics, Bethesda, MD 20814, USA.

[5] Uniformed Services University of the Health Sciences, Department of Gynecologic Surgery and Obstetrics, Bethesda, MD 20814, USA.

[#] These authors contributed equally

* To whom correspondence should be addressed:

Fereshteh S. Nugent, Ph.D., Edward Hebert School of Medicine, Department of Pharmacology, Uniformed Services University of the Health Sciences, 4301 Jones Bridge Road, Bethesda, Maryland 20814, fereshteh.nugent@usuhs.edu

Abstract

The lateral habenula (LHb), which plays a critical role in value-based decision-making and in stress responses, is linked to drug addiction and mood disorders. Prior research from our lab demonstrated the LHb's responsiveness to corticotropin-releasing factor (CRF), yet the origin of CRF inputs to this region remained elusive. Here, we mapped CRF projections to the LHb, revealing several contributing brain regions and a subpopulation of CRF-expressing LHb neurons (LHb^{CRF}) along with their downstream targets. Chemogenetic activation of LHb^{CRF} neurons did not affect conditioned place preference or anxiety-related behaviors in mice of either sex. However, it enhanced passive action-locking responses to a simulated aerial threat in both male and female mice as well as induced subtle sex-specific differences in escape latency which aligned with our observation of higher basal spontaneous activity in male LHb^{CRF} neurons. These findings indicate that LHb^{CRF} neurons can promote passive defensive responses to immediate danger, with baseline activity potentially influencing the timing of escape.

Introduction

The lateral habenula (LHb) is an evolutionarily conserved brain region crucial for behavioral selection, in response to stressors and rewards; thereby guiding goal-directed motivated behavior[1-3]. Ongoing research continues to unveil nuanced roles for the LHb in both normal behavior and the pathophysiology of mental illness. Aversive stimuli or the omission of expected reward generally activate the LHb, and its hyperactivity is implicated in anhedonic and negative states associated with depression, anxiety, and drug addiction. Conversely, reward-related stimuli inhibit LHb activity which generates positive motivational states. These findings highlight LHb's therapeutic potential, as evidenced by the anti-depressant effects of deep brain stimulation of the LHb and ketamine's NMDA receptor antagonism of LHb neurons [1-5].

The majority of LHb neurons are glutamatergic, and express markers such as the vesicular glutamate transporter 2 (VGLUT2) [6]. However, a small subset also expresses classical GABAergic markers, including glutamic acid decarboxylase 1 (GAD1), GAD2, the GABA transporter 1 (GAT-1), and the vesicular GABA transporter (VGAT), suggesting the presence of a functional intrinsic inhibitory circuit within the LHb[7-11]. Notably, some LHb neurons co-express both glutamatergic and GABAergic markers. For example, parvalbumin-expressing LHb neurons (LHb^{PV}) comprise three distinct subpopulations: a majority that are VGLUT2+ and glutamatergic, a subset that expresses only GABAergic markers, and a subpopulation that co-expresses both glutamatergic and GABAergic markers (e.g., VGLUT2 and GAD2)[7]. Most LHb glutamatergic outputs directly and indirectly modulate key monoaminergic systems, primarily the dopamine and serotonin pathways that encode behavioral avoidance and

reward prediction errors. Mechanistically, this involves suppressing dopamine release from the ventral tegmental area (VTA) and serotonin release from the raphe nuclei by exciting GABAergic neurons, particularly those in the rostromedial tegmental area (RMTg), thus shifting behavior away from reward-seeking[2, 12-14]. Consequently, LHb is increasingly recognized as a critical structure in the neural circuits that govern mood, motivation, and decision-making by processing a diverse array of appetitive and aversive signals that are crucial for adaptive behavior, allowing organisms to learn from both positive and negative experiences[5].

LHb neuronal activity is regulated by glutamatergic, GABAergic, and glutamate/GABA co-releasing synaptic inputs from various regions in the forebrain and midbrain such as the medial prefrontal cortex[15, 16], entopeduncular nucleus/globus pallidus[17, 18], lateral preoptic area (LPO) [29], ventral pallidum[19], lateral hypothalamus[20], ventromedial hypothalamus[16, 21, 22] , septum[23], central amygdala (CeA) [21], and bed nucleus of the stria terminalis (BNST)[21]. It also receives reciprocal inputs from the VTA[24], laterodorsal tegmental nucleus[25], periaqueductal gray (PAG)[15, 16], and locus coeruleus[1, 15] forming complex feedback loops that modulate activity. Given the widespread expression of various G protein-coupled receptors on LHb neurons and their afferents, LHb neuronal activity is subject to neuromodulatory actions of both fast and slow synaptic transmission from glutamate and GABA, as well as other neurotransmitters and neuromodulators including endocannabinoids[26], acetylcholine[27], serotonin[28-30], norepinephrine[31] and several co-released neuropeptides such as orexin[8], neuropeptide Y[32, 33], dynorphin[16, 34] and corticotropin-releasing factor (CRF)[35-38]. These diverse

glutamatergic, GABAergic, and neuromodulatory signals provide the LHb with information related to motivation, reward, aversion, and stress.

Specifically regarding CRF neuromodulatory actions, hypothalamic (paraventricular nucleus of hypothalamus, PVN) and extra-hypothalamic CRF systems mediate stress responses, and their dysfunction is implicated in stress-related disorders. CRF's central action through its receptors CRFR1/2 (both G protein-coupled receptors) is cell type-, region- and pathway-specific and depends on prior stress exposure[39]. Additionally, sex differences in CRF signaling may contribute to female vulnerability to anxiety and depression[40]. Our previous studies demonstrated that the rodent LHb is highly responsive to CRF[35, 36, 38], increasing LHb neuronal excitability via CRFR1-PKA-dependent suppression of different potassium currents (small conductance potassium SK channels in rat LHb[38]; M-type potassium channels in mouse LHb[35]). In rat LHb, CRF reduces presynaptic GABA release via retrograde endocannabinoid signaling, without changing glutamatergic activity, whereas in mouse LHb, CRF attenuates both GABAergic and glutamatergic transmission[35, 38]. We also showed that early life stress and brain trauma augment endogenous LHb CRF-CRFR1 signaling, contributing to LHb hyperexcitability[36, 38].

Building on these findings, here we investigated the source of CRF inputs to the LHb which remained unclear. Using viral-based Cre-mediated strategies in CRF transgenic mouse lines, we mapped LHb-projecting CRF neurons and discovered a previously uncharacterized neural subpopulation of LHb that express CRF (LHb^{CRF} neurons). We then traced the major downstream targets of LHb^{CRF} axonal projections, revealing both local and long-range projections to the midbrain. To identify the behavioral relevance of

these neurons, we used chemogenetic activation of LHb^{CRF} neurons which revealed their specific role in innate threat-evoked defensive behaviors, with sexual dimorphism in decision-making processing speed potentially linked to varying basal LHb^{CRF} activity in male and female mice.

Results

A subpopulation of CRF projections to the LHb originates within the LHb itself. To identify CRF projections to the LHb, we used Cre-dependent retrograde viral tracing by bilaterally injecting retrograde adeno-associated virus (rgAAV-DIO-YFP) into the LHb of CRH-Cre male and female mice (n=3). This revealed an intrinsic subpopulation of LHb neurons expressing CRF (LHb^{CRF}), in addition to CRF projections from the paraventricular nucleus of thalamus (PVT), and PAG (the main inputs) and smaller contributions from the PVN, BNST, and LPO (Figure 1). Notably, retrograde labeling was not detected in some other known CRF-expressing regions that project to the LHb, such as the VTA and CeA, supporting the rgAAV tracer's specificity. To determine if LHb^{CRF} neurons constitute a subclass of LHb^{PV} neurons, we also performed anti-parvalbumin immunostaining on retrogradely labeled LHb^{CRF} neurons. The absence of detectable parvalbumin expression in LHb^{CRF} neurons indicates that these are distinct subpopulations, separate from LHb^{PV} neurons. (Supplementary Figure 1).

LHb^{CRF} neurons express VGLUT2 but not VGAT mRNA. To further confirm and elucidate the neurochemical identity of LHb^{CRF} neurons, we used multiplex fluorescent in situ hybridization (RNAscope) to probe for CRH, VGLUT2, and VGAT mRNAs in LHb cell bodies, and assessed the overlap of VGLUT2 or VGAT with CRH mRNA to detect potential co-expression of these markers in adult mouse LHb (Figure 2). Similar to our

retrograde tracing study, we found that a subset of LHb neurons express CRH mRNA (Figure 2A-B). We also confirmed previous reports[1, 2] that the majority of LHb neurons express VLGUT2 (Figure 2C-F), and only a small minority express VGAT(Figure 2G-L). Importantly, 100% of CRH mRNA was colocalized with VGLUT2 mRNA, with no overlap with VGAT mRNA, demonstrating that LHb^{CRF} neurons are glutamatergic.

LHb^{CRF} neurons project locally within the LHb and to distant midbrain structures.

We next mapped the efferent projections of LHb^{CRF} neurons using Cre-dependent anterograde tracing with different viral vectors in male and female mice. Bilateral intra-LHb injections of AAV8-DIO-mCherry in 3 male mice (Figure 3) and AAV5-DIO-ChR2-YFP in 3 female mice (Figure 4) CRH-Cre mice revealed a comparable pattern of LHb^{CRF} axonal projections in both sexes. These projections targeted the LHb itself and midbrain structures such as the RMTg, PAG, and substantia nigra pars compacta (SNpc), suggesting a conserved fundamental organization of LHb^{CRF} circuitry across sexes.

Behavioral correlates of LHb^{CRF} neuronal activity

To establish causal links between LHb^{CRF} neuronal activity and behavior, we employed a Cre-dependent chemogenetic approach using excitatory Designer Receptors Exclusively Activated by Designer Drugs (DREADDs). Mice across multiple cohorts underwent behavioral testing (7-day intervals) in one of two sequences: light-dark test (LDT) followed by elevated zero maze (EZM), or open field test (OFT) followed by conditioned place preference (CPP) and then visual looming shadow test (VLST). The inclusion of EZM, LDT, and OFT was crucial for interpreting CPP and VLST data by controlling for potential non-specific effects of Gq-DREADD activation of LHb^{CRF}

neurons on locomotion and general anxiety. To selectively activate LHb neurons expressing CRF, we employed a Cre-dependent chemogenetic approach using two different constructs of DREADDs. In adult male and female CRH-Cre mice (postnatal day 42 [P42]), we performed bilateral stereotaxic injections into the LHb of an adeno-associated viral (AAV) vector encoding an excitatory Gq-coupled DREADD. Specifically, we utilized AAV8-hSyn-DIO-hM3D(Gq)-mCherry in CRH-Cre mice to drive Cre-dependent expression of hM3D(Gq) tagged with mCherry. Given the expression of the tdTomato reporter in CRH-Cre::Ai14 mice, we used an alternative Cre-dependent viral construct, AAV8-hSyn-DIO-HA-hM3D(Gq)-IRES-mCitrine, to avoid spectral overlap and ensure clear visualization of DREADD-expressing cells. To activate LHb^{CRF} neurons expressing Gq-DREADDs in CRH-Cre or CRH-Cre::Ai14 mice, mice received i.p. injections of 0.3mg/kg JHU37160 or vehicle (saline) 30 min prior to behavioral assay, at least four weeks post-surgery (consistent with our previous study[41]). During CPP conditioning, mice received JHU37160 or saline prior to the second of two daily conditioning sessions (days 2-3), but not during baseline evaluation (day 1) or testing (day 4). We confirmed that Gq-DREADD expression was restricted to the LHb^{CRF} neurons by mCherry expression or HA-hM3Dq staining and that bath application of JHU37160 (100nM) significantly increased neuronal excitability of LHb^{CRF} neuron expressing DREADD construct (Figures 5A-C and 6A-E).

Chemogenetic activation of LHb^{CRF} neurons did not induce anxiety-like or risk-taking behaviors. In EZM and LDT, mice generally prefer to spend more time in the closed arms of the EZM or the dark chamber of the LDT box. However, they may also be motivated to explore the open arms of the EZM or the bright area of the LDT

apparatus. Increased exploration of the open arms and light chamber is believed to reflect lower anxiety/more novelty seeking/risk-taking behaviors in mice. As shown in example traces of automated tracking of mouse movement in the EZM and LDT in Figure 5E-F, activation of LHb^{CRF} neurons by JHU37160 in CRH-Cre mice expressing Gq-DREADD did not alter time spent in the open arms of EZM or the light chamber of LDT [Figure 5G-I, EZM: Male (n=5-7/group); arm effect: F (1, 20) = 280.1, ****p<0.0001, JHU37160 effect: F (1, 20) = 0.031, p=0.86, arm x JHU37160 interaction: F (1, 20) = 0.34, p=0.56; Figure 5 J-L, EZM: Female (n=5-6/group); arm effect: F (1, 18) = 30.39, ****p<0.0001, JHU37160 effect: F (1, 18) = 0.00039, p=0.98, arm x JHU37160 interaction: F (1, 18) = 0.35, p=0.55; Figure 5M-O, LDT: Male (n=5-7/group); chamber effect: F (1, 20) = 98.61, ****p<0.0001, JHU37160 effect: F (1, 20) = 0.07734, p=0.78, chamber x JHU37160 interaction: F (1, 20) = 0.34, p=0.56; Figure 5P-R, LDT: Female (n=5-6/group); chamber effect: F (1, 18) = 34.68, ****p<0.0001, JHU37160 effect: F (1, 18) = 9.026e-005, p=0.99, chamber x JHU37160 interaction: F (1, 18) = 1.266, p=0.27, two-way ANOVA].

Chemogenetic activation of LHb^{CRF} neurons did not induce CPP. To control for Gq-DREADD effects on locomotor activity and general anxiety with EZM and LDT in CRH-Cre::Ai14 lines, we performed OFT where we consistently observed that chemogenetic excitation of LHb^{CRF} neurons by JHU37160 in CRH-Cre::Ai14 mice did not affect locomotor activity or promote anxiety-like behaviors in the OFT in either sex as shown in example traces in Figure 6F-G. CRH-Cre::Ai14 mice expressing Gq-DREADD injected with either JHU37160 or saline spent significantly less time in the center of the apparatus compared to the edges (periphery) and their total distance traveled was not

altered by our chemogenetic manipulation [Figure 6J-K, OFT: Male (n=10-12/group); region effect: F (1, 40) = 6656, ****p<0.0001, JHU37160 effect: F (1, 40) = 0.000, p=0.99, region x JHU37160 interaction: F (1, 40) = 0.018, p=0.89; Figure 6L-M, OFT: Female (n=9-10/group); region effect: F (1, 34) = 4476, ****p<0.0001, JHU37160 effect: F (1, 18) = 0.000, p=0.99, region x JHU37160 interaction: F (1, 34) = 0.5729, p=0.45, two-way ANOVA]. We then performed CPP to evaluate whether chemogenetic activation of LHb^{CRF} neurons is rewarding. We found that CRH-Cre::Ai14 mice expressing Gq-DREADD injected with JHU37160 during place conditioning spent equal time in JHU37160-paired and unpaired sides as seen in CRH-Cre::Ai14 mice expressing Gq-DREADD that received only saline during conditioning (Figure 6H-I and 6N-O).

Chemogenetic activation of LHb^{CRF} neurons promotes passive action-locking behavioral responses to threat. Finally, we tested whether chemogenetic activation of LHb^{CRF} neurons biases threat-evoked responses towards active (escape) or passive (action-locking/freezing) defensive behaviors and/or alters the latency to threat responses in mice (Figure 7A). We found that chemogenetic activation of LHb^{CRF} neurons by JHU37160 significantly increased action-locking/freezing responses in CRH-Cre::Ai14 male and female mice expressing Gq-DREADD compared to those injected with saline (Figure 7B and 7C, effect of JHU37160: *p<0.05, Chi squared tests) as well as prolonged the latency to initiate escape defensive behaviors in male but not female mice (Figure 7D and 7E, effect of JHU37160 in males: t=5.492, df=66, ****p<0.0001, Un-paired Student t-test).

LHb^{CRF} neurons exhibit higher baseline spontaneous activity in male mice compared to female mice. To further explore the cellular basis of sexually dimorphic behaviors mediating active escape in response to an aerial threat upon chemogenetic activation of LHb^{CRF} neurons, we further evaluated basal levels of spontaneous activity and neuronal excitability of LHb^{CRF} neurons (labeled with tdTomato) in CRH-Cre::Ai14 male and female mice (Figure 8A). We observed that male LHb^{CRF} neurons exhibited higher levels of spontaneous activity with more LHb^{CRF} neurons in tonic and bursting mode of activity than female LHb^{CRF} neurons (Figure 8B). In contrast, LHb^{CRF} neuronal excitability in response to depolarization did not differ between male and female CRH-Cre::Ai14 mice (Figure 8C) (Figure 8B, male: n=49 cells/22 mice, female: n=41 cells/9 mice in pie charts, *$p<0.05$, Chi squared tests; Figure 8C, male: n=42 cells/22 mice, female: n=30 cells/9 mice in excitability, effect of sex: $F(1, 740) = 0.096$, $p=0.75$, two-way ANOVA).

Discussion

The LHb's broad involvement in various adaptive behaviors and neuropsychiatric disorders, including depression, schizophrenia, Parkinson's disease, and attention-deficit hyperactivity disorder, continues to fuel significant clinical interest[42-50]. Despite displaying relatively uniform electrophysiological properties, LHb neurons exhibit substantial heterogeneity in their transcriptional profiles, afferents, and projections[6, 7, 51, 52]. Furthermore, neuromodulation profoundly shapes LHb neuronal activity through mechanisms such as the synaptic co-release of multiple neuromodulators alongside neurotransmitters, the expression of diverse neuromodulatory receptors, and the integration of various neuromodulatory signals, potentially contributing to the functional

specializations of distinct LHb neuron subpopulations[2]. Given this less explored facet of LHb function, and building on our previous demonstration of the LHb's responsiveness to the key stress neuromodulator CRF[35, 36, 38], we specifically investigated the origin of these previously uncharacterized CRF inputs to the LHb. Our investigation revealed several brain regions including a distinct subpopulation of LHb neurons that co-express glutamate and CRF (LHb^{CRF}), which could serve as a source of both local and distant neuromodulatory inputs to the LHb and the midbrain. Using chemogenetic activation of LHb^{CRF} neurons, we further demonstrate LHb^{CRF} neurons play a pivotal role in mediating passive defensive responses to imminent danger across sexes, with baseline activity potentially influencing active response timing.

Retrograde mapping in adult CRH-Cre mice identified the PAG, PVT, and the LHb itself as the major sources of CRF projections to the LHb, with minor contributions from the PVN, BNST, and LPO. It is important to note that while direct projections to the LHb from all other mentioned brain regions, as well as local excitatory and inhibitory connections within the LHb, are well-documented[1, 2, 9, 11, 53, 54], a direct anatomical connection from the PVT to the LHb has not been previously described. Although the absence of retrogradely-labeled CRF neurons in the VTA and CeA (known LHb afferents with CRF-containing neurons) supports the specificity of our CRF projection mapping, the lack of prior anatomical evidence for PVT-LHb connections underscores the need for careful further investigation to validate this finding and then explore the potential role of LHb-projecting PVT^{CRF} neurons. We then specifically focused on our newly discovered subpopulation of glutamatergic CRF-expressing LHb neurons (LHb^{CRF}), mapping their axonal projection targets and characterizing their behavioral

influences and physiological properties in male and female mice. Supporting this, our RNAscope analysis confirmed the existence of a subset of LHb neurons in the adult mouse brain that co-express VGLUT2 and CRH mRNAs, validating their glutamatergic identity. Using two distinct viral anterograde tracers in CRH-Cre mice, we also observed a consistent pattern of LHb^{CRF} axonal projections across both sexes. These projections included local circuits within the LHb and long-range projections to known LHb-projecting midbrain structures such as the RMTg, PAG, and SNpc[2, 55]. This conserved neural circuit architecture between males and females suggests that LHb^{CRF} neurons could mediate both a functional intrinsic microcircuit within the LHb and also provide neuromodulatory inputs to the PAG, RMTg, and SNpc. The expression of VGLUT2 in LHb^{CRF} neurons, coupled with the lack of parvalbumin expression, establishes that LHb^{CRF} neurons are a distinct subpopulation separate from LHb^{PV} neurons. This finding also excludes the possibility that LHb^{CRF} neurons are a component of the LHb^{PV} GABAergic interneurons responsible for local inhibition of glutamatergic neurons[11]. Our future research will focus on determining whether the intrinsic and extrinsic axonal terminals of LHb^{CRF} neurons form excitatory connections and co-release glutamate and CRF within the LHb, PAG, RMTg, and SNpc, as well as elucidate the behavioral significance of these circuits.

Our excitatory chemogenetic studies revealed a distinct role for LHb^{CRF} neurons in promoting passive action-locking/freezing responses to innately threatening looming stimuli in both male and female mice. Interestingly, we observed prolonged escape latencies in male, but not female, mice, which correlated with higher basal spontaneous activity of LHb^{CRF} neurons in males, characterized by a greater proportion of neurons

exhibiting tonic and bursting firing modes compared to females. In contrast, we found no sex-specific differences in overall LHb neuronal excitability in response to direct depolarization. This discrepancy may be specifically attributed to the significant increase in bursting activity of LHb^{CRF} neurons in males. Because depolarizing currents in excitability recordings typically elicit fewer action potentials per depolarization in bursting neurons compared to tonically active neurons, the higher proportion of bursting neurons with a lower firing rate in males could counteract the higher firing rate of tonically active neurons, resulting in similar overall neuronal excitability levels between sexes despite differences in basal spontaneous activities of LHb^{CRF} neurons.

Collectively, our findings point towards potentially stronger intrinsic and extrinsic glutamatergic outputs from LHb^{CRF} neurons in males, a characteristic that may underlie, at least in part, the sex-specific delayed escape responses observed in the looming shadow test following Gq-DREADD activation.

The hypothalamic PVN and specific extrahypothalamic CRF neurons, including the BNST (which we found both to provide weaker CRF projections to the LHb), are implicated in threat-driven defensive behaviors[56]. The looming shadow test also underscores the critical involvement of both LHb neurons[57] and PVN^{CRF} neurons[58] in threat-provoked defensive responses. This test exhibits strong face validity as the active fleeing (flight) or passive staying (action-locking/freezing) behaviors observed closely resemble human reactions to imminent danger. Importantly, dysregulation of these defensive mechanisms, such as rigid and persistent freezing or escape, and prolonged threat reactivity, are also key features of stress-related psychopathologies like anxiety and PTSD[59-64].

Fiber photometric recordings of PVN^{CRF} neurons in the looming shadow test demonstrated that augmented PVN^{CRF} neuronal activity precedes escape responses elicited by a looming or advancing threat[58]. Moreover, optogenetic inhibition of PVN^{CRF} neurons attenuates escape behavior[58]. Consequently, these findings suggest that PVN^{CRF} activity encodes an anticipatory or preparatory signal for the initiation of escape. Furthermore, distinct subpopulations of LHb neurons are involved in either predicting or reflecting the selection and execution of threat-driven action-locking or escape behaviors in the looming shadow test[57]. Fiber photometry of LHb population activity revealed an increase in calcium signal time-locked with escape and a decrease time-locked with action-locking. However, miniscope calcium imaging with single-cell resolution uncovered distinct LHb neuronal clusters: some increase their activity before and during escape while others decrease their activity before action-locking, while others increasing activity before action-locking while decreasing activity before escape. The former outcome is reminiscent of PVN^{CRF} neuron activity during this test. Our results suggest the possibility that LHb^{CRF} neurons represent a functionally distinct LHb subpopulation encoding action-locking defensive behaviors in response to an imminent threat. Future miniscope calcium imaging studies can further elucidate the role of LHb^{CRF} neurons and other LHb-projecting CRF neurons in the selection and execution of appropriate defensive responses. Our previous work also demonstrated that mild traumatic brain injury (mTBI) in male and female mice shifts threat responses towards action-locking in the looming shadow test, and prolongs escape latency in female mice specifically[36]. Considering that mTBI-induced LHb hyperactivity is partly driven by an increase in CRF-CRFR1 signaling within the LHb in both sexes, it is crucial to

investigate how LHb^{CRF} circuits contribute to the altered defensive behaviors observed after mTBI. Overall, our findings highlight that recruitment of LHb^{CRF} neuronal activity shifts mouse defensive behaviors towards action-locking in both sexes, with delayed defensive stress reactions only in males.

Curiously, our chemogenetic activation of LHb^{CRF} neurons did not alter place preference in either sex while activation of distinct subpopulations of CRF neurons could exert either place preference (e.g., NAc^{CRF} or CeA^{CRF} neurons) or aversion (e.g., $BNST^{CRF}$)[65]. One limitation of chemogenetic activation with sustained activation of LHb^{CRF} neurons is its lack of the millisecond-scale temporal precision offered by optogenetics. This limitation hinders a clear understanding of the immediate behavioral response to LHb^{CRF} neuronal stimulation. Therefore, future studies using behavioral assays like the real-time place preference paradigm could better address whether LHb^{CRF} neuronal stimulation evokes aversive (avoidance) or appetitive (approach) motivation. In summary, our work has unveiled a novel and previously uncharacterized subpopulation of LHb neurons forming both local and long-range CRF circuits projecting to the midbrain, implicating them in innate defensive behaviors. Further characterizing the precise functional connectivity and behavioral contributions of distinct LHb^{CRF} subpopulations based on their unique projection targets holds significant and timely impact. This is underscored by the established cell type-, region-, and pathway-specific nature of CRF neuromodulation across the brain, suggesting that dissecting these specific LHb^{CRF} circuits will provide critical insights into the nuanced roles of CRF in behavior.

Methods

Animals

Male and female mice, aged 9-13 weeks, were used for all experiments (viral injections at postnatal day 42 (P42); experiments commencing at 9 weeks of age). All procedures adhered to the NIH Guide for the Care and Use of Laboratory Animals and the ARRIVE guidelines 2.0, and were approved by the Uniformed Services University Institutional Animal Care and Use Committee. The following mouse strains were used: C57BL/6J (Strain #: 000664), n = 3; CRH-ires-CRE (B6(Cg)-*Crh*$^{tm1(cre)Zjh}$/J, Strain #: 012704), n = 32; CRH-Cre::Ai14 [generated by crossing homozygous CRH-ires-Cre mice (n=8 breeders) with Ai14 Cre reporter mice (n=8 breeders)(B6.Cg-*Gt(ROSA)26Sor*$^{tm14(CAG-tdTomato)Hze}$/J, Strain #: 007914)], n = 77. Mice were acquired from Jackson Laboratories at P35-P49 and allowed at least 72 hours of acclimation before experimental procedures began. Different numbers of male and female mice were used due to stock availability from the supplier and in-house breeding. Seven mice were excluded from chemogenetic studies due to incorrect LHb targeting. Mice were group-housed in standard cages under a 12hr/12hr light-dark cycle with standard laboratory lighting conditions (lights on, 0600-1800, ~200 lux), with ad libitum access to food and water. All procedures were performed 2-4 hours after the start of the light cycle. All efforts were made to minimize animal suffering and reduce the number of animals used throughout this study.

Virus injections for retrograde and anterograde tracings and chemogenetics

Mice (P42) were anesthetized with 1-3% isoflurane vaporized in oxygen and secured in a stereotaxic frame. Body temperature was maintained at 37°C throughout the procedure and during recovery using a heating pad. The scalp was shaved, and a midline incision was made to expose the skull. The following viral vectors were

bilaterally injected into the LHb: rgAAV-EF1a-DIO EYFP (Addgene #27056), AAV5-Ef1a-DIO hChR2(E123T/T159C)-EYFP (Addgene #35509), AAV8-hSyn-DIO-mCherry (Addgene #50459), AAV8-hSyn-DIO-hM3D(Gq)-mCherry (Addgene #44361), AAV8-hSyn-DIO-HA-hM4D(Gi)-IRES-mCitrine (Addgene #50455). Viral vectors (~50 nL/side) were infused at a rate of 1nL/sec over 5 minutes using a Nanoject III Injector (Drummond) and pulled glass pipettes into the LHb (coordinates from bregma: AP, -1.35 mm; ML, ±0.5 mm; DV, -3.0 mm). The injection pipette was left in place for 5 minutes post-infusion to allow for viral diffusion. During recovery (approximately 30-60 minutes), mice were placed in a warm cage (heating pad beneath) or under a heating lamp to prevent hypothermia. Post-operative care included continuous monitoring until purposeful movement was regained. Animal health and weight were monitored and recorded for at least 3 days post-surgery. Mice received a subcutaneous injection of 5 mg/kg carprofen (for analgesia) immediately after surgery and were monitored daily for signs of pain, with carprofen administered as needed. Viral expression was confirmed via fluorescence and/or immunohistochemistry at the conclusion of behavioral experiments. Mice lacking bilateral viral expression in the LHb were excluded from data analysis.

In situ hybridization (RNAscope)

RNAscope in situ hybridization was performed using the following probes from Advanced Cell Diagnostics (Newark, CA): Mm-Crh-C2 (mRNA encoding CRH), Mm-Slc32a1-C3 (mRNA encoding VGAT), Mm-Slc17a6 (mRNA encoding VGLUT2). The manufacturer's standard protocol for the RNAscope Fluorescent Multiplex Assay was followed for mouse brain tissues. Mice (C57Bl/6J) were anesthetized via intraperitoneal

injection of ketamine (85 mg/kg) and xylazine (10 mg/kg) and then perfused transcardially with 100 ml of 1x phosphate-buffered saline (PBS), followed by 200 ml of 4% paraformaldehyde (PFA) (Santa Cruz). Brains were dissected, post-fixed in 4% PFA for 24 hours, and cryoprotected in 20% sucrose for 3 days. Brains were then frozen on dry ice and stored at -80°C until sectioning. Coronal sections (20 μm) containing the LHb (from -0.94 to -2.3 mm caudal to bregma; Franklin and Paxinos, 2007) were cut using a cryostat (Leica CM1900) and mounted on slides. The multiplex fluorescent RNAScope assay (Advanced Cell Diagnostics) was performed as follows: sections baked in a 60° C oven, cooled, and then fixed in 4% PFA at 4°C for 1 hour and then dehydrated in increasing ethanol concentrations. Section were then treated with hydrogen peroxide followed by antigen retrieval. Finally, Protease III was applied to all sections. After each treatment, sections were washed in Nanopure water for 2 minutes (2x). RNA hybridization was performed using antisense probes against: Crh (316091; mRNA encoding mouse CRH), Slc17a6 (319171-C1; mRNA encoding VGLUT2), Slc32a1 (319191-C3; mRNA encoding VGAT) for 2 hours at 40°C. AMP's 1-3 were then applied and developed with the appropriate HRP conjugate followed by Vivid dye application (vivid dyes 520, 570, 650; 1:3000 dilution) and finally blocked. After each treatment sections were washed for 2 minutes in Wash Buffer. Sections were coverslipped using Prolong Gold with DAPI (Life Technologies, Eugene, OR). Images were acquired at 10x, 20x, and 40x magnification using a Leica DMRXA Fluorescence microscope or a Zeiss 980 Confocal Microscope.

Immunohistochemistry

At least three weeks following viral injection, similar to RNAScope procedure, mice were anesthetized and perfused transcardially and brain sections (20 μm) were cut using a cryostat, generating a series from Bregma 2.10 to -5.68mm AP. Sections were mounted on slides. For immunolabeling, LHb sections from CRH-Cre mice injected with rgAAV-EF1a-DIO EYFP (for parvalbumin staining) or CRH-Cre:Ai14 mice injected with AAV8-DIO-HA-hM3D(Gq)-mCitrine (for HA-tag staining) were blocked in 0.3% Triton X-100 containing 10% Normal Goat Serum (NGS) in 1x PBS for 1 hour and then incubated overnight at room temperature in carrier solution (5% NGS in 0.1% Triton X-100 in 1x PBS) with: mouse anti-parvalbumin IgG1 antibody (1:1000, Sigma, P3088) to detect parvalbumin expression in retrogradely labeled LHb^{CRF} neurons or rabbit anti-human influenza hemagglutinin (HA) antibody (1:500, Cell Signaling) to detect HA-hM3Dq in tdTomato-expressing LHb neurons.

Sections were rinsed in 1x PBS and incubated for 2 hours in Alexa Fluor® 594-labeled Goat anti-Mouse IgG1 or Alexa Fluor® 647-labeled Goat anti-Rabbit. Sections were rinsed again in 1x PBS and coverslipped with Prolong Gold mounting medium containing DAPI. Background staining was assessed by omitting the primary antibody (negative control). Brain tissue sections with known parvalbumin immunoreactivity (cortex, hippocampus) were also processed as positive control tissues. Images were captured using a Leica DMRXA Fluorescence microscope.

Quantification of retrogradely labeled CRF^+ neurons

For retrograde viral tracing quantification, labeled neurons were counted within regions of interest (ROIs) identified using the Allen Mouse Brain Atlas. Labeled cells were counted in each ROI across three consecutive sections, and the average number of

labeled cells per ROI was calculated. Data are presented as the percentage of labeled neurons within each ROI, calculated as (labeled neurons in ROI / total labeled neurons across all ROIs) × 100. CRF^+ neurons were quantified using tissue from three CRH-Cre mice.

Slice Preparation

Electrophysiology experiments were performed using CRH-Cre::Ai14 male and female mice. Mice were anesthetized with isoflurane and decapitated. Brains were rapidly dissected and placed in ice-cold artificial cerebrospinal fluid (ACSF) containing (in mM): 126 NaCl, 21.4 $NaHCO_3$, 2.5 KCl, 1.2 NaH_2PO_4, 2.4 $CaCl_2$, 1.00 $MgSO_4$, 11.1 glucose, 0.4 ascorbic acid; saturated with 95% O_2-5% CO_2. Sagittal slices (220 μm) containing the LHb were cut using a vibratome (Leica; Wetzlar, Germany) and incubated in the ACSF at 34°C for at least 1 hour prior to recording. Slices were transferred to a recording chamber and perfused with ascorbic-acid-free ACSF at 28-30°C.

Electrophysiology

Whole-cell recordings were performed on LHb-containing slices using patch pipettes (3-6 MΩ) and a patch amplifier (MultiClamp 700B) under infrared-differential interference contrast microscopy. Data acquisition and analysis were performed using DigiData 1440A, pCLAMP 10 (Molecular Devices), Clampfit, and GraphPad Prism 10. Signals were filtered at 3 kHz and digitized at 10 kHz. Cell input resistance and series resistance were monitored throughout the experiment. Data were excluded if these values changed by more than 10%. LHb slices were perfused with ascorbic-acid-free ACSF and patched with potassium gluconate-based internal solution (130 mM K-

gluconate, 15 mM KCl, 4 mM ATP-Na+, 0.3 mM GTP-Na+, 1 mM EGTA, and 5 mM HEPES, pH adjusted to 7.28 with KOH, osmolarity adjusted to 275-280 mOsm). Spontaneous neuronal activity and action potential (AP) firing patterns (tonic, bursting) were assessed in cell-attached recordings in voltage-clamp mode at V=0 for ~1 minute. For excitability assessment, LHb neurons were given increasingly depolarizing current steps (5-second duration) at +10 pA intervals, ranging from +10 pA to +100 pA. Neurons were maintained at -65 to -70 mV with manual direct current injection between pulses (20-second interstimulus interval). The number of APs generated by each depolarization step was counted and averaged for each experimental group.

Behavioral assays with chemogenetics

Four weeks post-viral injections, behavioral testing began with separate cohorts of CRH-Cre or CRH-Cre::Ai14 male and female mice expressing Gq DREADD in LHb. Mice received intraperitoneal injections of either 0.3mg/kg of the DREADD ligand, JHU37160, or vehicle (equivalent volumes of 0.9% saline) 30 min prior to behavioral testing, consistent with our previous study[41]. In the CPP test, DREADD-injected mice underwent conditioning with JHU37160 paired with either the preferred or non-preferred side of the chamber in a balanced (unbiased) manner. In these cohorts, JHU37160 or saline was administered only during conditioning days (days 2-3), not during habituation (day 1) or testing (day 4).

Open field test (OFT)

Mice were placed in an open field arena (40 cm x 40 cm) with dim white lighting (~5lux) and allowed to explore freely for 15 minutes. Animal movement was tracked using Any-

Maze video tracking software (Stoelting Co.), recording distance traveled and time spent in the periphery and center zones.

Elevated zero maze (EZM)

To assess anxiety and risk-taking behavior, mice were placed in an elevated zero maze and allowed to freely explore for 10 minutes with dim white lighting (~5lux). The maze, elevated 40 cm above the floor, comprises a ring-shaped arena with four arms (5 cm x 30 cm): two enclosed arms with 20-cm high walls and two open arms. An overhead camera and Any-Maze software (Stoelting Co.) were used to track the animal's movement, quantifying the number of entries and the time spent in both the open and closed arms, along with the total distance traveled.

Light-Dark Test (LDT)

The light-dark box test, similar in concept to the elevated zero maze but without the height factor, consists of a 40 cm x 40 cm box divided into a dark, enclosed chamber and a bright, exposed chamber (~750lux). While mice prefer the dark chamber, they also explore the bright area. Less time spent in the light chamber and more time in the dark is interpreted as higher anxiety. An overhead camera and Any-Maze software (Stoelting Co.) tracked the animal's position, recording distance traveled and time spent in each chamber.

Conditioned place preference (CPP)

We employed a three-compartment apparatus to conduct CPP testing. This apparatus featured outer compartments with distinct visual cues (e.g., circles vs. triangles walls) and a small central compartment lacking specific cues. Gates allowed mice to freely traverse the three compartments. Anymaze software was used to track the time spent in

each compartment during the pre-test, conditioning, and test phases. The CPP procedure comprised: Pretest (Day 1): To assess baseline preferences, each mouse was placed in the central compartment and allowed to explore all three compartments for 20 minutes. Conditioning (Days 2-3): Mice underwent conditioning sessions wherein they were confined to one outer compartment and administered saline, followed by confinement to the opposite compartment (after a >4-hour interval) and administration of either saline or JHU37160 (30 minutes prior to confinement). The pairing of saline or JHU37160 with a specific compartment was balanced across animals. Test (Day 4): Mice were given free access to all compartments, and the time spent in the saline/JHU37160-paired compartment was measured to determine place preference. Place preference was quantified by calculating a preference score: time spent in the saline/JHU37160-paired compartment during the post-test minus time spent in that compartment during the pre-test (post-pre).

Looming-shadow test

This test simulates a predator threat to induce defensive behaviors in mice, which manifest as either passive action-locking/freezing or active escape. The testing environment consisted of a 17 x 10 x 8.5-inch plastic arena with a 21-inch LCD monitor positioned overhead to present the visual stimulus. A 6 x 6 x 3-inch shelter was placed on one side of the arena. Behavior was recorded with a camera positioned laterally above the arena. First, mice were habituated to the arena for two days (10 minutes/day). On the test day, there was a 5-minute habituation period within the arena before stimulus presentation and then mice were presented with five looming visual stimuli, with at least a 1-minute inter-trial interval. The stimulus comprised of a 2-cm

black disk expanding to 20 cm over 9 seconds, divided into three phases: 2 seconds at 2 cm, 5 seconds of expansion, and 2 seconds at 20 cm. Defensive responses were classified as: escape (active movement to the shelter) and action-locking/freezing (absence of movement or repeated, discontinuous freezing). Mice were excluded as non-responders if they exhibited no discernible reaction to the looming stimulus (no freezing, no behavioral change, and failure to reach the shelter within 8 seconds). Video recordings were used to blindly score the type of defensive behavior and the latency to escape.

Statistics and reproducibility

Data are presented as mean ± SEM. Statistical significance was assessed using unpaired two-tailed Student's t-tests, Chi-square tests, and two-way ANOVA with Bonferroni post hoc tests. A significance threshold of $P < 0.05$ was used for all analyses. Statistical analyses were performed using GraphPad Prism 10.

Data availability

Data supporting the conclusions of this study are available from the corresponding author upon reasonable request.

References

1. Hu H, Cui Y, Yang Y. Circuits and functions of the lateral habenula in health and in disease. Nat Rev Neurosci. 2020;21(5):277-95; doi: 10.1038/s41583-020-0292-4
2. Groos D, Helmchen F. The lateral habenula: A hub for value-guided behavior. Cell reports. 2024;43(4):113968; doi: https://doi.org/10.1016/j.celrep.2024.113968
3. Baker PM, Mathis V, Lecourtier L, et al. Lateral Habenula Beyond Avoidance: Roles in Stress, Memory, and Decision-Making With Implications for Psychiatric Disorders. Front Syst Neurosci. 2022;16:826475; doi: 10.3389/fnsys.2022.826475
4. Proulx CD, Hikosaka O, Malinow R. Reward processing by the lateral habenula in normal and depressive behaviors. Nature neuroscience. 2014;17(9):1146-52; doi: 10.1038/nn.3779
5. Wang D, Li Y, Feng Q, et al. Learning shapes the aversion and reward responses of lateral habenula neurons. eLife. 2017;6:e23045; doi: 10.7554/eLife.23045

6. Hashikawa Y, Hashikawa K, Rossi MA, et al. Transcriptional and Spatial Resolution of Cell Types in the Mammalian Habenula. Neuron. 2020;106(5):743-58 e5; doi: 10.1016/j.neuron.2020.03.011
7. Nguyen TVT, Nakamura T, Ichijo H. Topographic Organization of Glutamatergic and GABAergic Parvalbumin-Positive Neurons in the Lateral Habenula. eNeuro. 2024;11(7); doi: 10.1523/ENEURO.0069-24.2024
8. Flanigan ME, Aleyasin H, Li L, et al. Orexin signaling in GABAergic lateral habenula neurons modulates aggressive behavior in male mice. Nature neuroscience. 2020;23(5):638-50; doi: 10.1038/s41593-020-0617-7
9. Zhang L, Hernandez VS, Swinny JD, et al. A GABAergic cell type in the lateral habenula links hypothalamic homeostatic and midbrain motivation circuits with sex steroid signaling. Translational psychiatry. 2018;8(1):50; doi: 10.1038/s41398-018-0099-5
10. Webster JF, Lecca S, Wozny C. Inhibition Within the Lateral Habenula-Implications for Affective Disorders. Front Behav Neurosci. 2021;15:786011; doi: 10.3389/fnbeh.2021.786011
11. Webster JF, Vroman R, Balueva K, et al. Disentangling neuronal inhibition and inhibitory pathways in the lateral habenula. Sci Rep. 2020;10(1):8490; doi: 10.1038/s41598-020-65349-7
12. Quina LA, Tempest L, Ng L, et al. Efferent Pathways of the Mouse Lateral Habenula. Journal of Comparative Neurology. 2015;523(1):32-60; doi: https://doi.org/10.1002/cne.23662
13. Zahm DS, Root DH. Review of the cytology and connections of the lateral habenula, an avatar of adaptive behaving. Pharmacology, biochemistry, and behavior. 2017;162:3-21; doi: 10.1016/j.pbb.2017.06.004
14. Hong S, Jhou TC, Smith M, et al. Negative reward signals from the lateral habenula to dopamine neurons are mediated by rostromedial tegmental nucleus in primates. J Neurosci. 2011;31(32):11457-71; doi: 10.1523/JNEUROSCI.1384-11.2011
15. Mathis VP, Williams M, Fillinger C, et al. Networks of habenula-projecting cortical neurons regulate cocaine seeking. Science Advances. 2021;7(45):eabj2225; doi: doi:10.1126/sciadv.abj2225
16. Flerlage WJ, Simmons SC, Thomas EH, et al. Dysregulation of kappa opioid receptor neuromodulation of lateral habenula synaptic function following a repetitive mild traumatic brain injury. Pharmacology Biochemistry and Behavior. 2024;243:173838; doi: https://doi.org/10.1016/j.pbb.2024.173838
17. Wallace ML, Saunders A, Huang KW, et al. Genetically Distinct Parallel Pathways in the Entopeduncular Nucleus for Limbic and Sensorimotor Output of the Basal Ganglia. Neuron. 2017;94(1):138-52 e5; doi: 10.1016/j.neuron.2017.03.017
18. Li H, Pullmann D, Jhou TC. Valence-encoding in the lateral habenula arises from the entopeduncular region. Elife. 2019;8; doi: 10.7554/eLife.41223
19. Liu B, Cao Y, Wang J, et al. Excitatory transmission from ventral pallidum to lateral habenula mediates depression. World J Biol Psychiatry. 2020;21(8):627-33; doi: 10.1080/15622975.2020.1725117
20. Lecca S, Meye FJ, Trusel M, et al. Aversive stimuli drive hypothalamus-to-habenula excitation to promote escape behavior. Elife. 2017;6; doi: 10.7554/eLife.30697

21. Liu X, Huang H, Zhang Y, et al. Sexual Dimorphism of Inputs to the Lateral Habenula in Mice. Neuroscience bulletin. 2022;38(12):1439-56; doi: 10.1007/s12264-022-00885-y
22. Golden SA, Heshmati M, Flanigan M, et al. Basal forebrain projections to the lateral habenula modulate aggression reward. Nature. 2016;534(7609):688-92; doi: 10.1038/nature18601
23. Zhang GW, Shen L, Zhong W, et al. Transforming Sensory Cues into Aversive Emotion via Septal-Habenular Pathway. Neuron. 2018;99(5):1016-28.e5; doi: 10.1016/j.neuron.2018.07.023
24. Root DH, Mejias-Aponte CA, Zhang S, et al. Single rodent mesohabenular axons release glutamate and GABA. Nature neuroscience. 2014;17(11):1543-51; doi: 10.1038/nn.3823
25. Lima LB, Bueno D, Leite F, et al. Afferent and efferent connections of the interpeduncular nucleus with special reference to circuits involving the habenula and raphe nuclei. The Journal of comparative neurology. 2017;525(10):2411-42; doi: 10.1002/cne.24217
26. Hwang EK, Zapata A, Hu V, et al. Basal forebrain-lateral habenula inputs and control of impulsive behavior. Neuropsychopharmacology. 2024;49(13):2060-8; doi: 10.1038/s41386-024-01963-7
27. Wolfe CIC, Hwang E-K, Ijomor EC, et al. Muscarinic Acetylcholine M₂ Receptors Regulate Lateral Habenula Neuron Activity and Control Cocaine Seeking Behavior. The Journal of Neuroscience. 2022;42(28):5552-63; doi: 10.1523/jneurosci.0645-22.2022
28. Fu R, Mei Q, Shiwalkar N, et al. Anxiety during alcohol withdrawal involves 5-HT2C receptors and M-channels in the lateral habenula. Neuropharmacology. 2020;163:107863; doi: 10.1016/j.neuropharm.2019.107863
29. Zuo W, Zhang Y, Xie G, et al. Serotonin stimulates lateral habenula via activation of the post-synaptic serotonin 2/3 receptors and transient receptor potential channels. Neuropharmacology. 2016;101:449-59; doi: 10.1016/j.neuropharm.2015.10.012
30. Shabel SJ, Proulx CD, Trias A, et al. Input to the lateral habenula from the Basal Ganglia is excitatory, aversive, and suppressed by serotonin. Neuron. 2012;74(3):475-81; doi: 10.1016/j.neuron.2012.02.037
31. Root DH, Hoffman AF, Good CH, et al. Norepinephrine activates dopamine D4 receptors in the rat lateral habenula. J Neurosci. 2015;35(8):3460-9; doi: 10.1523/JNEUROSCI.4525-13.2015
32. Cheon M, Park H, Chung C. Protein kinase C mediates neuropeptide Y-induced reduction in inhibitory neurotransmission in the lateral habenula. Neuropharmacology. 2020;180:108295; doi: https://doi.org/10.1016/j.neuropharm.2020.108295
33. Cheon M, Park H, Rhim H, et al. Actions of Neuropeptide Y on Synaptic Transmission in the Lateral Habenula. Neuroscience. 2019;410:183-90; doi: 10.1016/j.neuroscience.2019.04.053
34. Simmons SC, Shepard RD, Gouty S, et al. Early life stress dysregulates kappa opioid receptor signaling within the lateral habenula. Neurobiol Stress. 2020;13:100267; doi: 10.1016/j.ynstr.2020.100267
35. Simmons SC, Flerlage WJ, Langlois LD, et al. AKAP150-anchored PKA regulates synaptic transmission and plasticity, neuronal excitability and CRF

neuromodulation in the mouse lateral habenula. Communications Biology. 2024;7(1):345; doi: 10.1038/s42003-024-06041-8
36. Flerlage WJ, Simmons SC, Thomas EH, et al. Effects of Repetitive Mild Traumatic Brain Injury on Corticotropin-Releasing Factor Modulation of Lateral Habenula Excitability and Motivated Behavior. J Neurotrauma. 2024; doi: 10.1089/neu.2024.0184
37. Zuo W, Zuo Q, Wu L, et al. Roles of corticotropin-releasing factor signaling in the lateral habenula in anxiety-like and alcohol drinking behaviors in male rats. Neurobiol Stress. 2021;15:100395; doi: 10.1016/j.ynstr.2021.100395
38. Authement ME, Langlois LD, Shepard RD, et al. A role for corticotropin-releasing factor signaling in the lateral habenula and its modulation by early-life stress. Science signaling. 2018;11(520); doi: 10.1126/scisignal.aan6480
39. Henckens MJ, Deussing JM, Chen A. Region-specific roles of the corticotropin-releasing factor-urocortin system in stress. Nat Rev Neurosci. 2016;17(10):636-51; doi: 10.1038/nrn.2016.94
40. Bangasser DA, Wiersielis KR. Sex differences in stress responses: a critical role for corticotropin-releasing factor. Hormones. 2018;17(1):5-13; doi: 10.1007/s42000-018-0002-z
41. Flerlage WJ, Langlois LD, Rusnak M, et al. Involvement of Lateral Habenula Dysfunction in Repetitive Mild Traumatic Brain Injury-Induced Motivational Deficits. J Neurotrauma. 2023;40(1-2):125-40; doi: 10.1089/neu.2022.0224
42. Lawson RP, Nord CL, Seymour B, et al. Disrupted habenula function in major depression. Molecular psychiatry. 2017;22(2):202-8; doi: 10.1038/mp.2016.81
43. Weidacker K, Kim S-G, Nord CL, et al. Avoiding monetary loss: A human habenula functional MRI ultra-high field study. Cortex. 2021;142:62-73; doi: https://doi.org/10.1016/j.cortex.2021.05.013
44. Abraham ME, Ong V, Gendreau J, et al. Investigating Deep Brain Stimulation of the Habenula: A Review of Clinical Studies. Neuromodulation: Technology at the Neural Interface. 2023;26(2):292-301; doi: https://doi.org/10.1016/j.neurom.2022.05.005
45. Samanci B, Tan S, Michielse S, et al. The habenula in Parkinson's disease: Anatomy, function, and implications for mood disorders − A narrative review. Journal of chemical neuroanatomy. 2024;136:102392; doi: https://doi.org/10.1016/j.jchemneu.2024.102392
46. Proulx CD, Hikosaka O, Malinow R. Reward processing by the lateral habenula in normal and depressive behaviors. Nature neuroscience. 2014;17(9):1146-52; doi: 10.1038/nn.3779
47. Arfuso M, Salas R, Castellanos FX, et al. Evidence of Altered Habenular Intrinsic Functional Connectivity in Pediatric ADHD. J Atten Disord. 2021;25(5):749-57; doi: 10.1177/1087054719843177
48. Lee Y-A, Goto Y. The Habenula in the Link Between ADHD and Mood Disorder. Frontiers in Behavioral Neuroscience. 2021;15; doi: 10.3389/fnbeh.2021.699691
49. Lawson RP, Drevets WC, Roiser JP. Defining the habenula in human neuroimaging studies. NeuroImage. 2013;64:722-7; doi: https://doi.org/10.1016/j.neuroimage.2012.08.076

50. Zhu Y, Qi S, Zhang B, et al. Connectome-Based Biomarkers Predict Subclinical Depression and Identify Abnormal Brain Connections With the Lateral Habenula and Thalamus. Frontiers in psychiatry. 2019;10; doi: 10.3389/fpsyt.2019.00371
51. Wallace ML, Huang KW, Hochbaum D, et al. Anatomical and single-cell transcriptional profiling of the murine habenular complex. Elife. 2020;9; doi: 10.7554/eLife.51271
52. Cerniauskas I, Winterer J, de Jong JW, et al. Chronic Stress Induces Activity, Synaptic, and Transcriptional Remodeling of the Lateral Habenula Associated with Deficits in Motivated Behaviors. Neuron. 2019;104(5):899-915 e8; doi: 10.1016/j.neuron.2019.09.005
53. Zhang L, Hernandez VS, Vazquez-Juarez E, et al. Thirst Is Associated with Suppression of Habenula Output and Active Stress Coping: Is there a Role for a Non-canonical Vasopressin-Glutamate Pathway? Frontiers in neural circuits. 2016;10:13; doi: 10.3389/fncir.2016.00013
54. Margolis EB, Fields HL. Mu Opioid Receptor Actions in the Lateral Habenula. PLoS One. 2016;11(7):e0159097; doi: 10.1371/journal.pone.0159097
55. Quina LA, Tempest L, Ng L, et al. Efferent pathways of the mouse lateral habenula. The Journal of comparative neurology. 2015;523(1):32-60; doi: 10.1002/cne.23662
56. Chudoba R, Dabrowska J. Distinct populations of corticotropin-releasing factor (CRF) neurons mediate divergent yet complementary defensive behaviors in response to a threat. Neuropharmacology. 2023;228:109461; doi: 10.1016/j.neuropharm.2023.109461
57. Lecca S, Namboodiri VMK, Restivo L, et al. Heterogeneous Habenular Neuronal Ensembles during Selection of Defensive Behaviors. Cell reports. 2020;31(10):107752; doi: 10.1016/j.celrep.2020.107752
58. Daviu N, Füzesi T, Rosenegger DG, et al. Paraventricular nucleus CRH neurons encode stress controllability and regulate defensive behavior selection. Nature neuroscience. 2020;23(3):398-410; doi: 10.1038/s41593-020-0591-0
59. Bastos AF, Vieira AS, Oliveira JM, et al. Stop or move: Defensive strategies in humans. Behavioural brain research. 2016;302:252-62; doi: https://doi.org/10.1016/j.bbr.2016.01.043
60. Sippel LM, Taverna E, Marshall AD. In vivo defensive behaviors, fear, and attention bias to physical and negative evaluation threats. Behaviour Research and Therapy. 2022;154:104108; doi: https://doi.org/10.1016/j.brat.2022.104108
61. Roelofs K, Hagenaars MA, Stins J. Facing Freeze: Social Threat Induces Bodily Freeze in Humans. Psychological Science. 2010;21(11):1575-81; doi: 10.1177/0956797610384746
62. Roelofs K. Freeze for action: neurobiological mechanisms in animal and human freezing. Philosophical transactions of the Royal Society of London. 2017;372(1718); doi: 10.1098/rstb.2016.0206
63. Kearney BE, Lanius RA. The brain-body disconnect: A somatic sensory basis for trauma-related disorders. Frontiers in neuroscience. 2022;16:1015749; doi: 10.3389/fnins.2022.1015749
64. Sege CT, Bradley MM, Lang PJ. Avoidance and escape: Defensive reactivity and trait anxiety. Behav Res Ther. 2018;104:62-8; doi: 10.1016/j.brat.2018.03.002

65. Baumgartner HM, Schulkin J, Berridge KC. Activating Corticotropin-Releasing Factor Systems in the Nucleus Accumbens, Amygdala, and Bed Nucleus of Stria Terminalis: Incentive Motivation or Aversive Motivation? Biological psychiatry. 2021;89(12):1162-75; doi: 10.1016/j.biopsych.2021.01.007

Acknowledgements: The opinions and assertions contained herein are the private opinions of the authors and are not to be construed as official or reflecting the views of the Uniformed Services University of the Health Sciences or the Department of Defense or the Government of the United States. This work was supported by the National Institute of Mental Health (NIH/NIMH) Grant# R21 MH132136 to FSN. The funding agency did not contribute to writing this article or deciding to submit it. We gratefully acknowledge the Preclinical Behavior and Modeling Core for providing access to and support with their behavioral equipment, which was essential for the successful completion of this study.

Author contributions: FSN and WJF designed the study. WJF, SCS, and EHT performed electrophysiology. TJW, SCG, and EHT were responsible for breeding CRH-Cre::Ai14 mice. SCG performed RNAscope and immunohistochemistry, with assistance from LI and EP for RNAscope optimization. SCG, SCS, and WJF conducted viral stereotaxic injections. WJF, EHT, MCT, and SCS carried out chemogenetic behavioral assays. Data analysis and figure preparation were performed by WJF, SCG, SCS, EHT, OLR, and FSN. The initial manuscript draft was written by WJF, SCG, EHT, EP, BMC, and FSN. All authors critically reviewed and approved the final version of the manuscript.

Competing interests: The authors declare no conflict of interest.

Figure Legends:

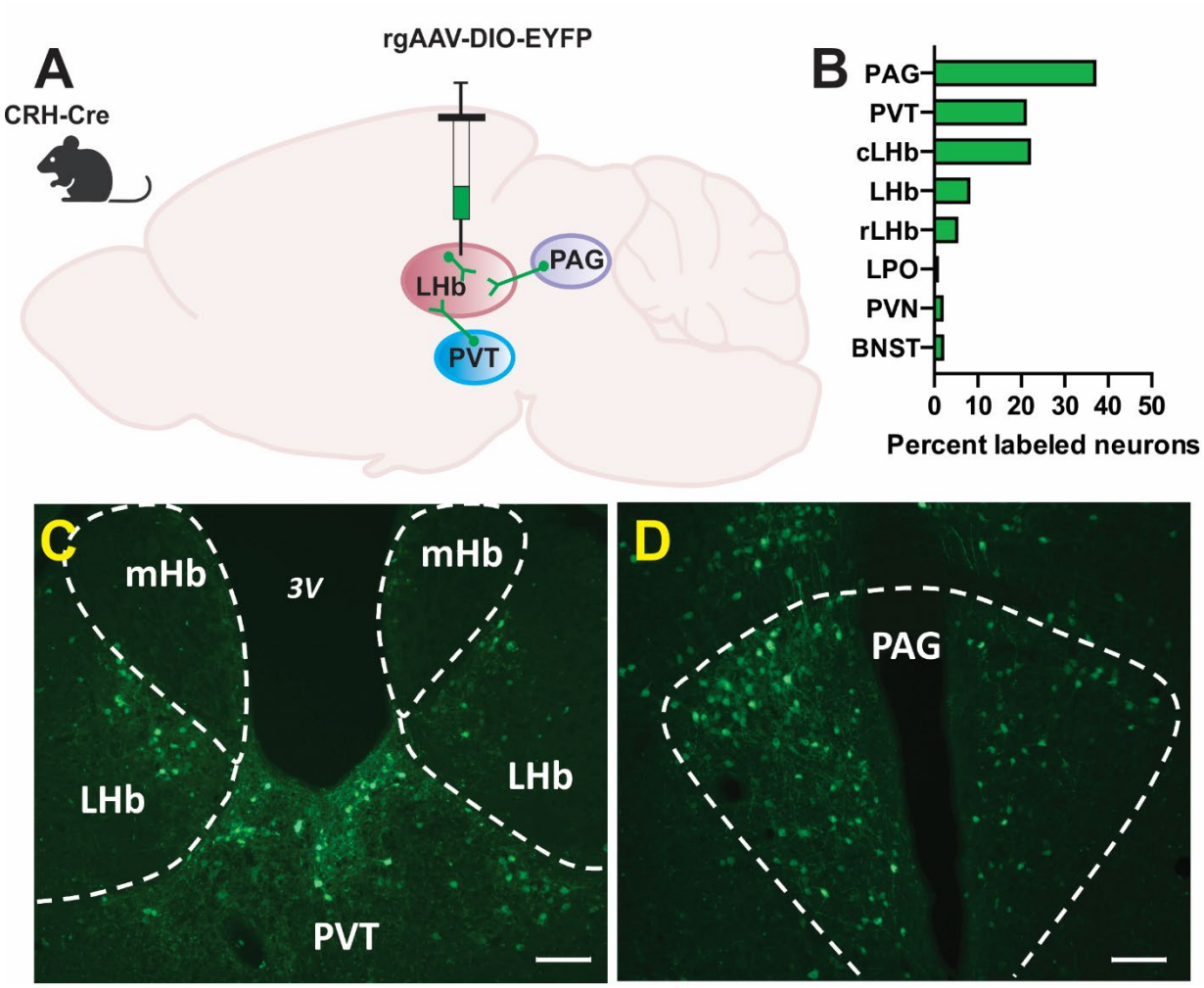

Figure 1: Retrograde viral tracing to identify brain regions that send CRF-expressing (CRF⁺) inputs to the lateral habenula (LHb) in mice. A illustrates the experimental design: a virus (rAAV-DIO-YFP) was injected into the LHb of CRF-Cre mice to label cells projecting to the LHb that also express CRF. **B** quantifies retrogradely labeled cell bodies (green) across brain sections. For each region of interest (ROI), cells were counted in three consecutive sections (Bregma ± 0.12mm), averaged across 3 mice (2 males and 1 female), and expressed as a percentage of total labeled cells (n=361). **C-D** show representative images of the labeling. The following ROIs were analyzed: BNST (bed nucleus of the stria terminalis, Bregma -0.1), PVN

(paraventricular hypothalamic nucleus, Bregma -0.82), LPO (lateral preoptic area, Bregma -0.1), rLHb (rostral lateral habenula, Bregma -1.22), LHb (lateral habenula, Bregma -1.58), cLHb (caudal lateral habenula, Bregma -1.94), PVT (paraventricular thalamic nucleus, Bregma -1.84), PAG (periaqueductal gray, Bregma -2.7), Scale bar = 100μm

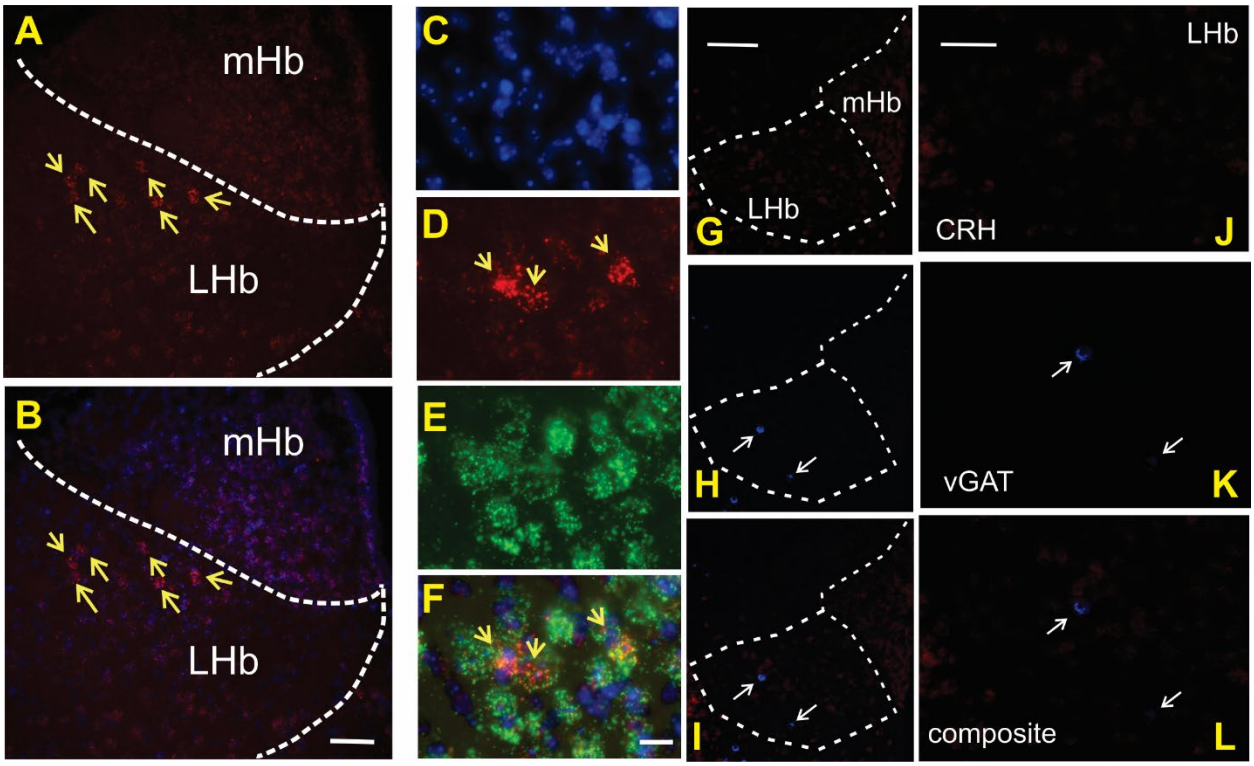

Figure 2. Mouse LHb^{CRF} neurons express VGLUT2 mRNA and are glutamatergic. **A-B** show fluorescence microscopy images of CRH mRNA (red) in the LHb of a C57BL/6 mouse, counterstained with DAPI (blue). Yellow arrows indicate CRF^{+} neurons. Scale bar = 25 μm. **C-F** show confocal microscopy images of CRH (red) and VGLUT2 (green) mRNAs, counterstained with DAPI (blue), in the LHb of a C57BL/6 mouse. Yellow arrows indicate co-localization of CRF and VGLUT2. Scale bar = 25 μm. **G-L** show fluorescence microscopy images of CRH (red) and VGAT (blue) mRNAs in the LHb of a C57BL/6 mouse at low (G-I, Scale bar = 100 μm) and high (J-L, Scale bar = 50 μm) magnification. White arrows indicate VGAT^{+} neurons, which do not express CRH mRNA. Abbreviations: medial habenula (mHb), lateral habenula (LHb).

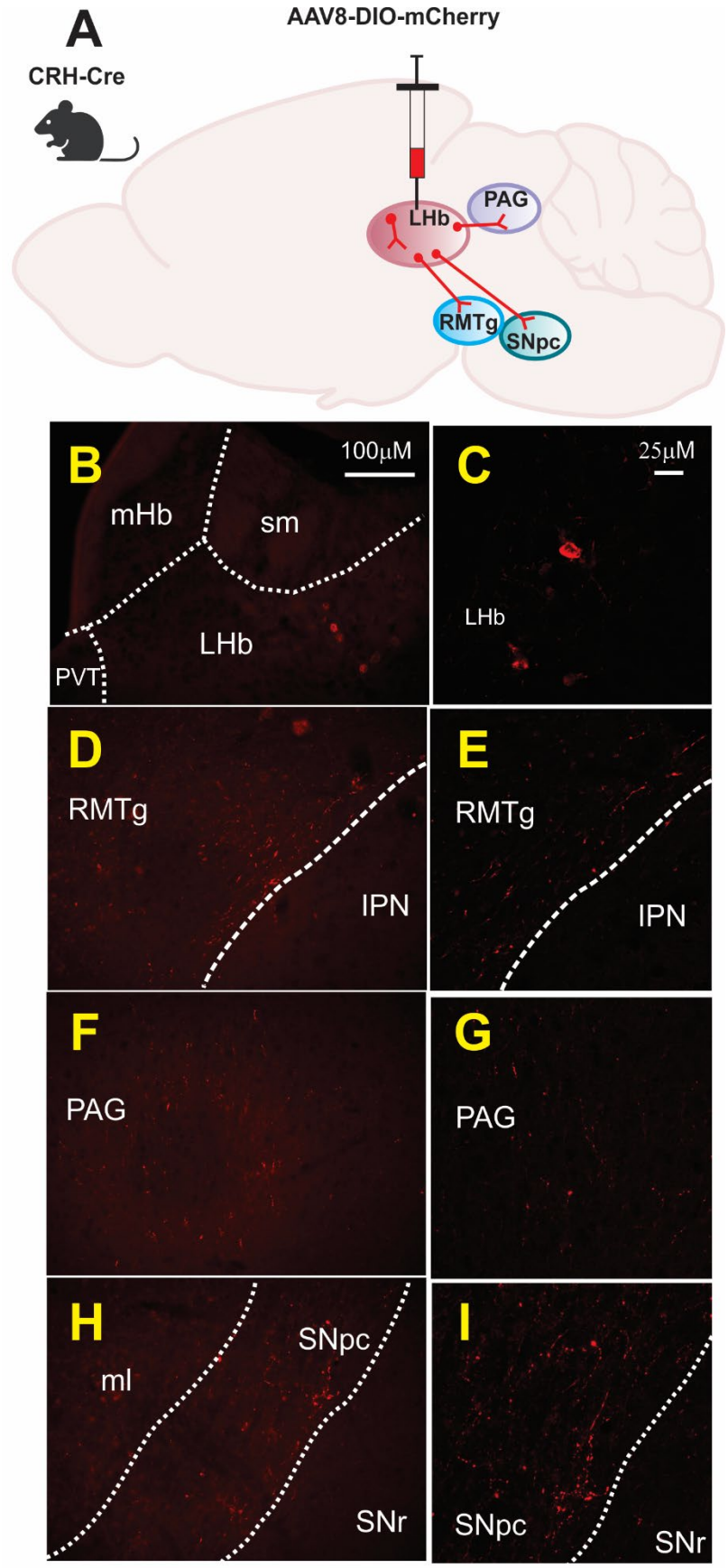
A
CRH-Cre
AAV8-DIO-mCherry
LHb
PAG
RMTg
SNpc
B
100μM
mHb
sm
LHb
PVT
C
25μM
LHb
D
RMTg
IPN
E
RMTg
IPN
F
PAG
G
PAG
H
ml
SNpc
SNr
I
SNpc
SNr

Figure 3. Anterograde viral tracing of LHb^{CRF} neuronal projections in CRH-Cre male mice. A shows a schematic of AAV8-DIO-mCherry injection into the LHb of a CRH-Cre male mice (n=3). **B-I** show representative low (left) and high (right) magnification fluorescent and confocal microscopy images of mCherry-labeled processes of LHb^{CRF} neurons found within the LHb itself, rostromedial tegmental area (RMTg), periaqueductal grey (PAG) and substantia nigra pars compacta (SNpc) in CRH-Cre male mice. Abbreviations: interpeduncular nucleus (IPN), medial habenula (mHb), medial lemniscus (ml), paraventricular nucleus of thalamus (PVT), stria medullaris (sm), substantia nigra pars reticulata (SNr).

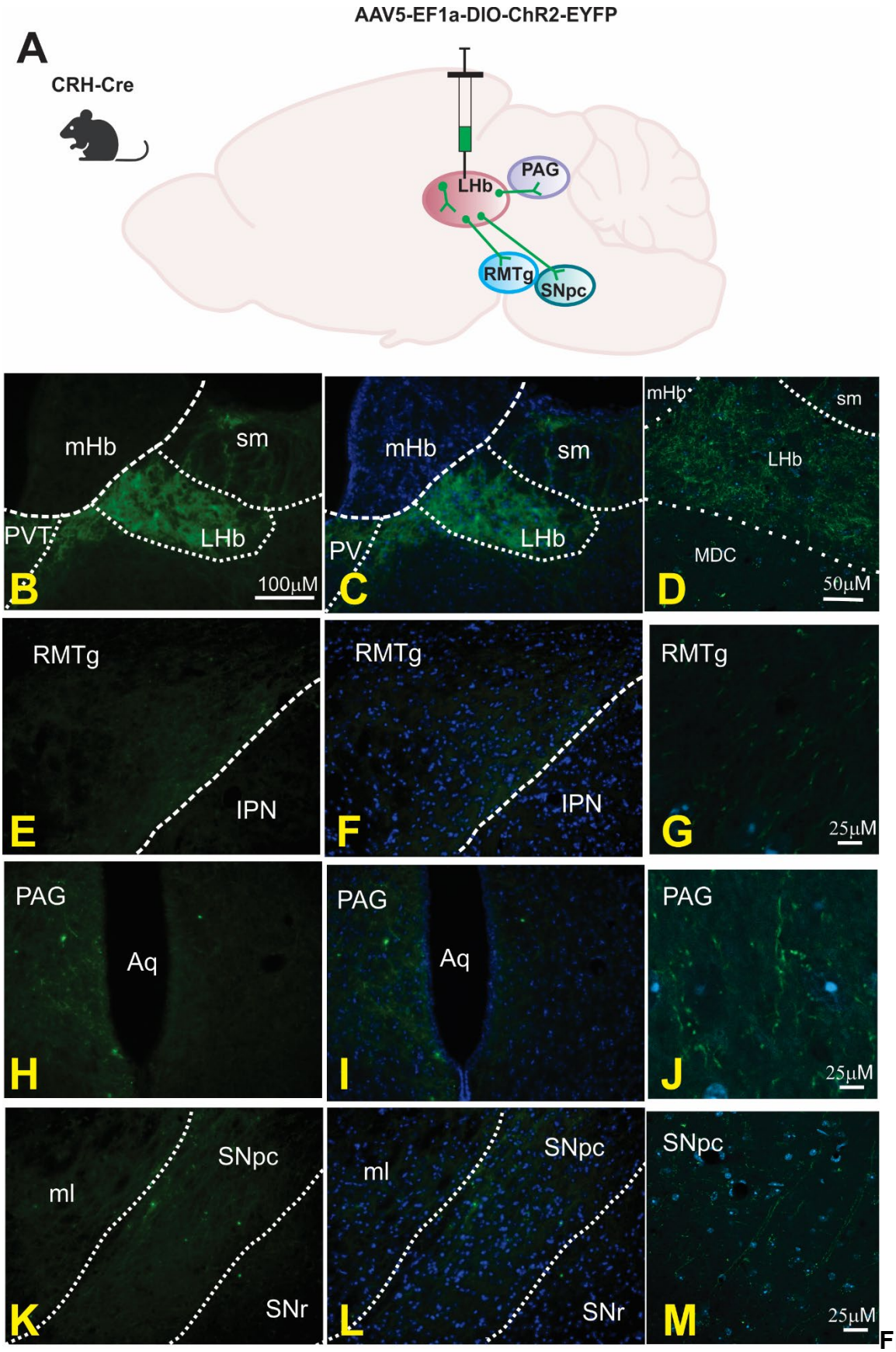
AAV5-EF1a-DIO-ChR2-EYFP
A
CRH-Cre
LHb
PAG
RMTg
SNpc
mHb
sm
PVT
LHb
B
100μM
mHb
sm
PV
LHb
C
mHb
sm
LHb
MDC
D
50μM
RMTg
IPN
E
RMTg
IPN
F
RMTg
G
25μM
PAG
Aq
H
PAG
Aq
I
PAG
J
25μM
ml
SNpc
SNr
K
ml
SNpc
SNr
L
SNpc
M
25μM

Figure

4. Anterograde viral tracing of LHb^{CRF} neuronal projections in CRH-Cre female mice. A shows a schematic of AAV5-DIO-ChR2-YFP injection into the LHb of a CRH-Cre female mice (n=3). **B-M** show representative low (LHb: B-C, RMTg: E-F, PAG: H-I, SNpc: K-L) and high (LHb: D, RMTg: G, PAG: J, SNpc: M) magnification fluorescent and confocal microscopy images of ChR2-YFP-labeled processes of LHb^{CRF} neurons found within the LHb itself, rostromedial tegmental area (RMTg), periaqueductal grey (PAG) and substantia nigra pars compacta (SNpc) in CRH-Cre female mice. Abbreviations: aqueduct (Aq), interpeduncular nucleus (IPN), medial habenula (mHb), medial lemniscus (ml), mediodorsal nucleus of thalamus (MDC), paraventricular nucleus of thalamus (PVT), stria medullaris (sm), substantia nigra pars reticulata (SNr).

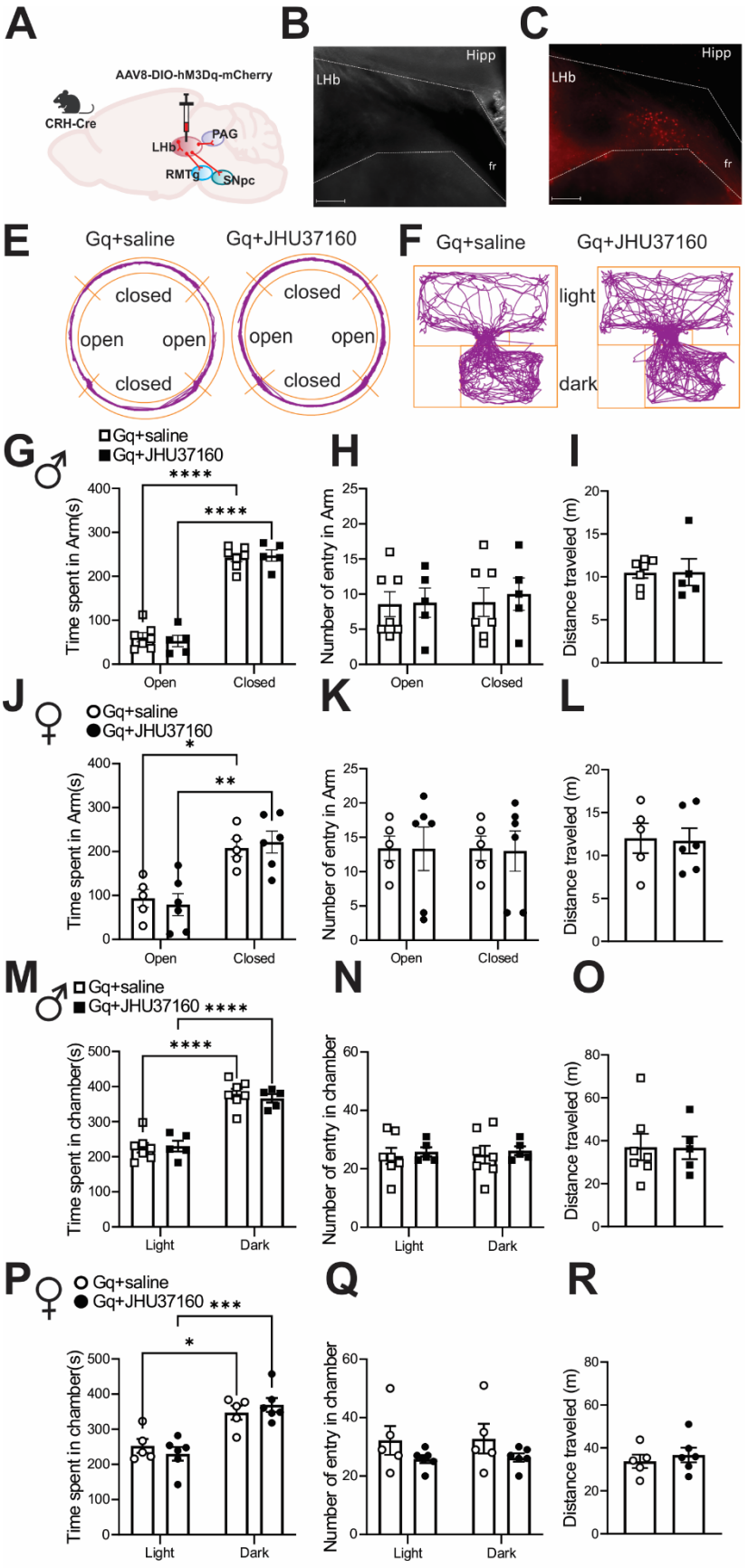
A
AAV8-DIO-hM3Dq-mCherry
CRH-Cre
LHb
PAG
RMTg
SNpc
B
Hipp
LHb
fr
C
Hipp
LHb
fr
E
Gq+saline
Gq+JHU37160
closed
open
open
closed
closed
open
open
closed
F
Gq+saline
Gq+JHU37160
light
dark
G
Gq+saline
Gq+JHU37160
Time spent in Arm(s)
Open
Closed
H
Number of entry in Arm
Open
Closed
I
Distance traveled (m)
J
Gq+saline
Gq+JHU37160
Time spent in Arm(s)
Open
Closed
K
Number of entry in Arm
Open
Closed
L
Distance traveled (m)
M
Gq+saline
Gq+JHU37160
Time spent in chamber(s)
Light
Dark
N
Number of entry in chamber
Light
Dark
O
Distance traveled (m)
P
Gq+saline
Gq+JHU37160
Time spent in chamber(s)
Light
Dark
Q
Number of entry in chamber
Light
Dark
R
Distance traveled (m)

Figure 5: Chemogenetic activation of LHb^{CRF} neurons did not affect locomotor activity or anxiety-related behavior in the elevated zero maze (EZM) or light-dark box (LDT). A Schematic depicting AAV8-DIO-hM3Dq-mCherry injection into the LHb of a CRH-Cre mouse. **B-C** Representative images of a sagittal LHb slice from a CRH-Cre mouse injected with Gq-DREADD, visualized using IR-DIC (**B**) and fluorescence (**C**) microscopy. **E-F** Representative track plots illustrating the movement of mice in the EZM (**E**) and LDT (**F**) following saline or JHU37160 injection. **G-L** Quantification of EZM behavior, showing no difference between JHU37160- and saline-injected mice of either sex in time spent in open arms, number of entries to open arms, or total distance traveled. **M-R** Quantification of LDT behavior, showing no difference between JHU37160- and saline-injected mice of either sex in time spent in light chambers, number of entries to light chambers, or total distance traveled. *$p<0.05$, **$p<0.01$, ***$p<0.001$, ****$p<0.0001$; 2way-ANOVA.

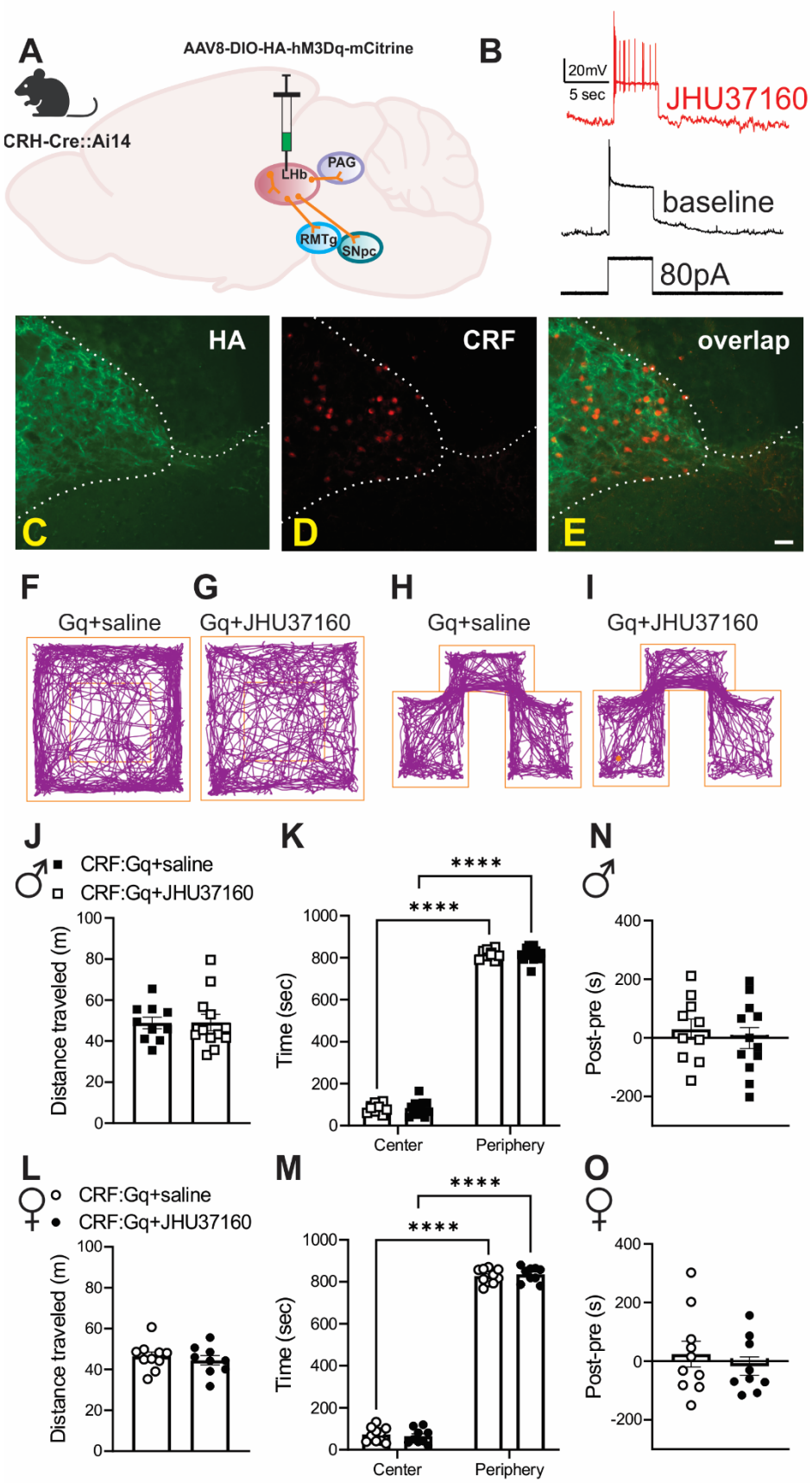
A
AAV8-DIO-HA-hM3Dq-mCitrine
CRH-Cre::Ai14
LHb
PAG
RMTg
SNpc
B
20mV
5 sec
JHU37160
baseline
80pA
HA
CRF
overlap
C
D
E
F
Gq+saline
G
Gq+JHU37160
H
Gq+saline
I
Gq+JHU37160
J
CRF:Gq+saline
CRF:Gq+JHU37160
Distance traveled (m)
K
Time (sec)
Center
Periphery
****
****
N
Post-pre (s)
L
CRF:Gq+saline
CRF:Gq+JHU37160
Distance traveled (m)
M
Time (sec)
Center
Periphery
****
****
O
Post-pre (s)

Figure 6: Chemogenetic activation of LHb^{CRF} neurons failed to elicit changes in locomotor activity or anxiety-like behavior in the open field test (OFT) and did not induce place preference or aversion in the conditioned place preference Test (CPP). A Injection schematic: AAV8-DIO-HA-hM3Dq-mCherry into the LHb of a CRH-Cre::Ai14 mouse. **B** Representative traces of action potential generation in response to an 80pA current step in an LHb^{CRF} neuron expressing hM3Dq+ before and after bath application of 100 nM JHU37160. **C-E** Fluorescent images of a coronal LHb section from a CRH-Cre::Ai14 mouse injected with AAV-DIO-HA-hM3Dq, stained with anti-HA antibody, confirming co-expression of tdTomato (red) and HA-hM3Dq (green) in LHb^{CRF} neurons. **F-I** Representative track plots showing mouse movement in the OFT (**F-G**) and in the saline-/JHU37160-paired and unpaired compartments of the CPP (**H-I**) for saline- or JHU37160-injected CRH-Cre::Ai14 Gq-DREADD mice. **J-K** and **L-M** Quantification of OFT performance revealed no significant differences between JHU37160- and saline-treated mice of either sex in total distance traveled or time spent in the center or periphery of the arena. **N-O** CPP analysis showed no evidence of place preference in JHU37160-paired CRH-Cre::Ai14 Gq-DREADD mice, comparable to saline-paired ones.

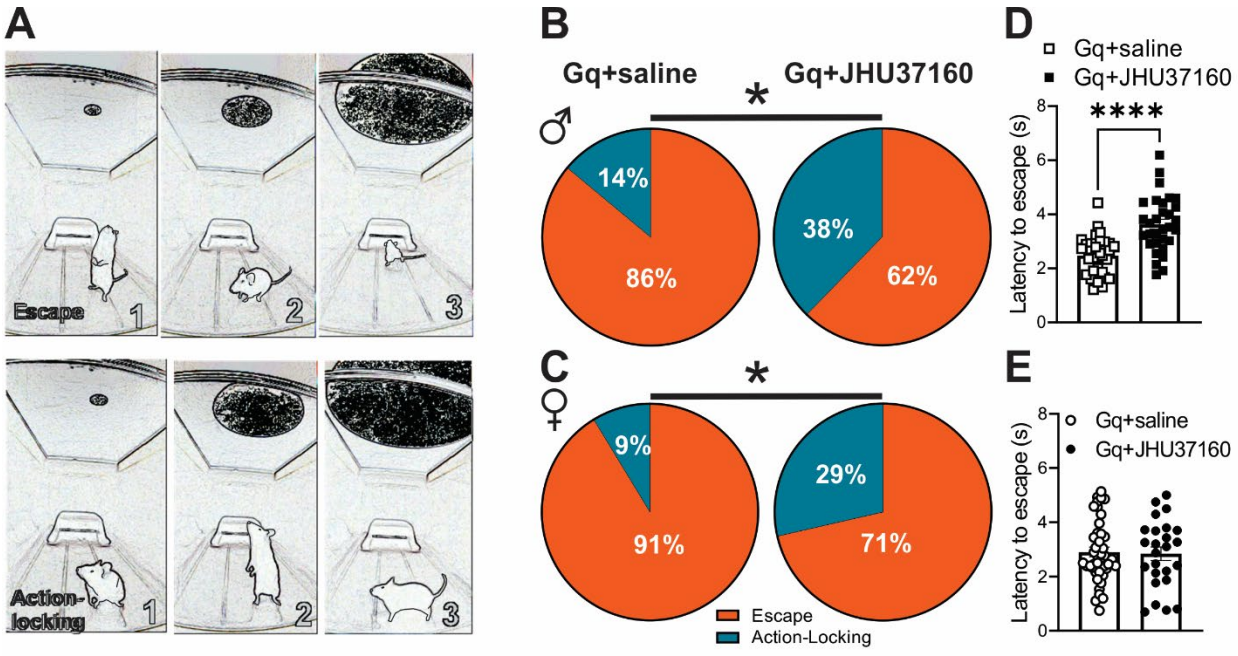

Figure 7: Chemogenetic activation of LHb^{CRF} neurons enhances passive action-locking responses in the visual looming shadow test (VLST). A Schematic illustrating mouse defensive behavior s, escape and action-locking, in the VLST. **B-C** The percent distribution of action-locking (teal blue) and escape (orange) behaviors in response to a looming shadow threat in male (B) and female (C) CRH-Cre::Ai14 Gq-DREADD mice receiving either saline or JHU37160. **D-E** Escape response latencies to a looming shadow threat in male (D) and female (E) CRH-Cre::Ai14 Gq-DREADD mice administered saline or JHU37160. *p<0.05, Chi-square test, Student's t-test; *****p<0.0001.

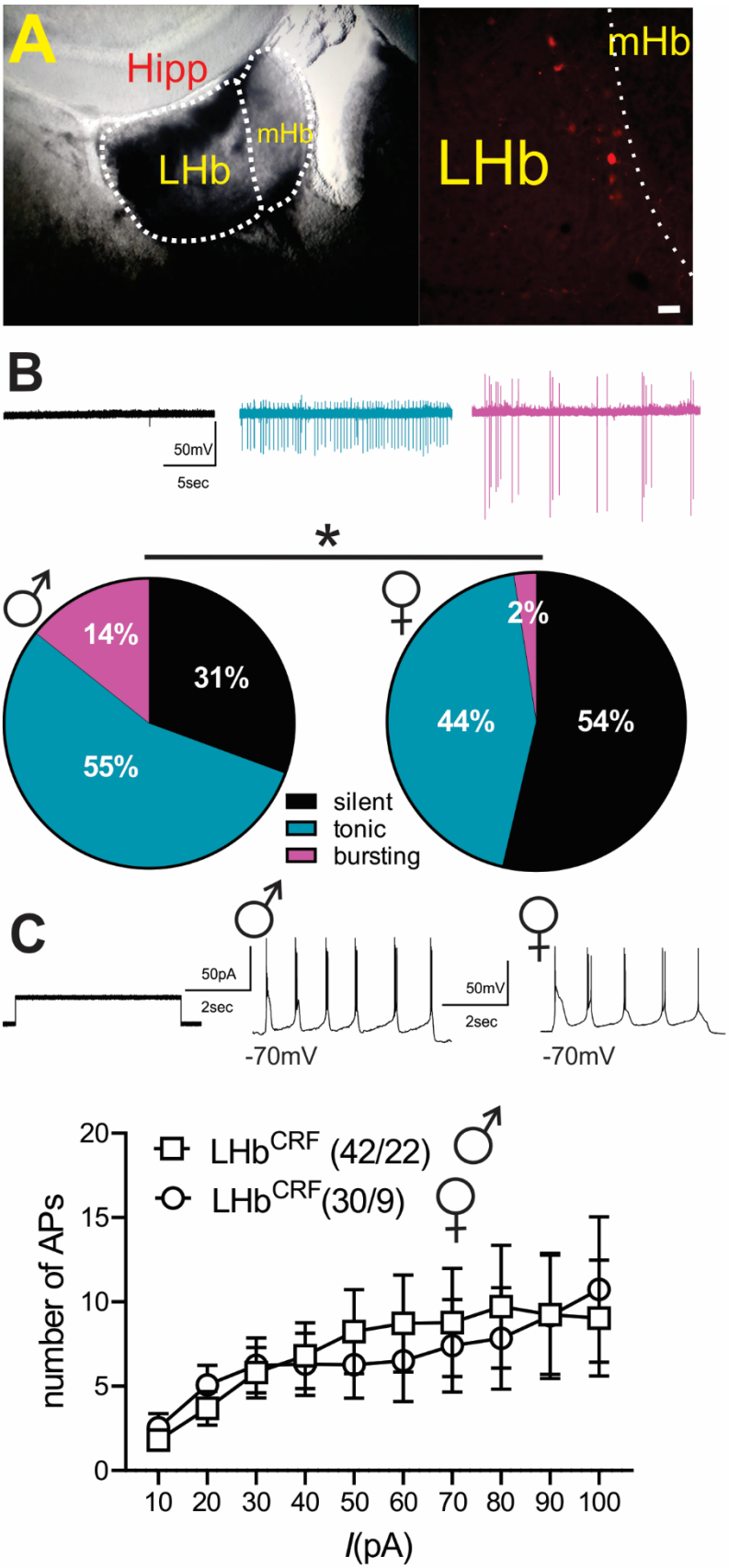
A
Hipp
mHb
LHb
mHb
LHb
B
50mV
5sec
*
14%
31%
55%
2%
44%
54%
silent
tonic
bursting
C
50pA
2sec
50mV
2sec
-70mV
-70mV
LHb^CRF (42/22)
LHb^CRF(30/9)
number of APs
0
5
10
15
20
10 20 30 40 50 60 70 80 90 100
I(pA)

Figure 8: LHb^{CRF} neurons in male CRH-Cre::TdTomato mice exhibit greater spontaneous tonic and bursting activity than in females. A Coronal habenula slice images from a CRH-Cre::tdTomato mouse, visualized using IR-DIC (left) and fluorescence (right; scale bar = 40 μm). **B** Representative traces and pie charts illustrating spontaneous neuronal activity and the percentage of silent (black), tonic (blue), or bursting (pink) activity patterns in tdTomato-labeled LHb^{CRF} neurons from male (n=49 cells/22 mice) and female (n=41 cells/9 mice) CRH-Cre::TdTomato mice (voltage-clamp, cell-attached recordings at V=0 mV). **C** Action potential (AP) generation in response to depolarizing current steps in tdTomato-labeled LHb^{CRF} neurons, recorded under conditions of intact synaptic transmission, with representative traces from male (black open squares, n=42 cells/22 mice) and female (black open circles, 30 cells/9 mice) CRH-Cre::TdTomato mice. *$p<0.05$; Chi-square test.

Supplemental Figure 1: Distinction between mouse LHb^{CRF} and LHb^{PV} neurons. A-C Representative images showing retrogradely labeled LHb^{CRF} neurons (green), parvalbumin immunostaining (red) using an anti-parvalbumin antibody, and the merged image, to determine if parvalbumin-expressing LHb neurons (LHb^{PV}) also express CRF in the mouse LHb.